J. Electroanal. Chem., 114 (1980) 89—115

POLYMER FILMS ON ELECTRODES

PART III. DIGITAL SIMULATION MODEL FOR CYCLIC VOLTAMMETRY OF ELECTROACTIVE POLYMER FILM AND ELECTROCHEMISTRY OF POLY(VINYLFERROCENE) ON PLATINUM

PAMELA J. PEERCE * and ALLEN J. BARD **

Department of Chemistry, The University of Texas at Austin, Austin, TX 78712 (U.S.A.)

(Received 6th May 1980)

ABSTRACT

The electrochemistry of electrodeposited poly(vinylferrocene) (PVF) and poly(vinylferrocene acrylonitrile) (PVFAN) films on platinum electrodes was studied in acetonitrile solutions using perchlorate or *p*-toluenesulfonate as the counter ion by cyclic voltammetry. A model is proposed for the cyclic voltammetric behavior of polymeric films on electrode surfaces. The model incorporates non-equivalent redox sites with interconversion between such sites, electron-transfer kinetics at substrate/film interface and diffusion within the film. Parameters are obtained which yield a good fit to the experimental results.

INTRODUCTION

The reversible electrochemical oxidation and reduction of electroactive polymers on electrode surfaces has been reported by a number of groups [1—8]. At scan rates less than about 1 V s^{-1}, the cyclic voltammetric waves have often shown behavior which approximated that expected of surface-confined reactants [9]: symmetrical shape [1,3,5a,6b—e,7b,8]; proportionality of the peak current with scan rate, v [1,3,4b,5a—b,6a—d,7,8]; and small separation between the peak potentials of the anodic and cathodic waves (ΔE_p) [1,3—8]. However, behavior suggestive of mass transport limitations has been noted at higher scan rates [4], especially for relatively thick films (Γ, surface concentration of redox centers, $\geqslant 10^{-8}$ mol cm^{-2}), and even with thinner films ($\Gamma \sim 10^{-11}$—10^{-9} mol cm^{-2}) [1c,1e,7]. This behavior was observed at scan rates >1 V s^{-1} when the temperature was lowered [1f], the size of the counter ion was increased [6d] or a less swelling solvent was employed [1d,1i].

Although symmetrical waves have been observed, their shapes often deviate from those expected of surface species, and the half-height peak widths ($\Delta E_{1/2}$) have been found to be equal to the theoretical surface confined species value of 90.6 mV (25°C) for a one-electron process in only a few cases [1d,7b,8]; more frequently, they range from 150 to 540 mV. This broadening of the surface

* Present address: Occidental Research Corp., P.O. Box 19601, Irvine, CA 92713, U.S.A.
** To whom correspondence should be addressed.

waves has been attributed to repulsive interactions [1d,1g,1h,1j], differences in the spatial distribution of the redox centers [5a,7a] and a distribution of species with different E^0 values for the electroactive groups [6d]. Wrighton and co-workers reported the occasional occurrence of two distinct oxidation for ferrocene bound to gold electrodes [6d].

The existence of electrochemically non-equivalent sites in polymer films on electrode surfaces is supported by the results with poly(hydroxymethylferrocene methacrylate) [5a]. Complex voltammetric waves also have been reported for poly(phenoxytetrathiafulvalene) [7b]. Asymmetric surface waves have also been reported [1c,1i,4,5,7b] which suggest interactions and differences in the surface activities of the two redox states of the polymers; for example, half-widths <<90.6 mV have been observed [1i,5,7b]. Daum and Murray found that the $\Delta E_{1/2}$ of the anodic peak for thin films of plasma polymerized vinylferrocene decreased from ca. 150 mV in acetonitrile to 18 mV in water and attributed the narrowing to the nearly constant activity of the ferricenium sites in water, a low swelling solvent [1i]. Kaufman and co-workers effected a substantial sharpening of the waves for the $TTF^{2+}/TTF^{\cdot+}$ couple by reducing the size of the counter ion and ascribed this effect to the more rapid dimerization of the TTF radical cations in the presence of the smaller anion [7b].

Peak potential separations in excess of 60 mV have been reported at higher scan rates [1c,1e,4a]. Such ΔE_p values >60 mV are generally indicative of slow electron transfer between the electrode and the redox centers in the polymer film, but they can also be caused by film (or solution) resistance effects. Measurement of the rate of heterogeneous electron transfer to a polymer film has not yet been reported.

Methods for evaluating heterogeneous rate constants for surface reactions by cyclic voltammetry which take account of the lateral interactions between the adsorbed species have been proposed [10]. Unfortunately, such procedures cannot be applied directly to the determination of rate constants for most polymer films because they neglect mass transport problems inherent in multilayer surface films, the possible presence of electrochemically non-equivalent redox sites and any changes in the extent of swelling or structure which occur upon oxidation and reduction (e.g. differences in the properties of the charged and neutral films).

In this paper, we propose a model for the oxidation and reduction of electronically non-conductive surface and calculate the current—potential characteristics by digital simulation techniques. The effect of the factors discussed above on the electrochemistry of the surface films is examined and the simulated results are compared to the experimental data for electrodeposited poly(vinylferrocene) (PVF) films in 0.1 *M* tetra-*n*-butylammonium perchlorate (TBAP)/MeCN solutions over a wide range of scan rates.

EXPERIMENTAL

Materials

Acetonitrile (MeCN) (Mahteson, Coleman and Bell), methylene chloride (CH_2Cl_2) (Fischer) and tetra-*n*-butylammonium perchlorate (TBAP) (South-

western Analytical Chemicals) were purified as previously described [5c]. Tetraethylammonium *p*-toluenesulfonate (TEAPTS) (Eastman) was dried on the vacuum line for several days. Azoisobis(butyronitrile) (AIBN) (Pfaltz-Bauer) was recrystallized once from methanol and air dried. Vinylferrocene (Strem Chemicals) was sublimed once and air dried. Acrylonitrile (Eastman) was distilled under vacuum.

Poly(vinylferrocene) was prepared by the method of Chen et al. which was reported to yield a polymer of molecular weight approximately 50,000 [11]. The preparation of the nearly ideally alternating copolymer of PVF, poly-(vinylferrocene acrylonitrile) (PVFAN) [12], followed a similar procedure except that an equimolar amount of degassed acrylonitrile was also injected into the polymerization tube containing the vinylferrocene and AIBN after it had been thoroughly purged with nitrogen.

Apparatus

All solution preparation and electrochemical experiments were performed in a Vacuum Atmosphere Co. glove box under a helium atmosphere. The cells and electrochemical instrumentation used have been previously described [5c]. A platinum disk electrode (area = 0.035 cm^2) was used as the working electrode and a coiled piece of platinum wire served as the auxiliary electrode. Potentials were measured and are reported with respect to a silver wire quasi-reference electrode whose potential was 50 ± 10 mV negative of the aqueous SCE. Positive feedback techniques were employed to compensate for solution resistance. All measurements were performed at the laboratory temperature, 25 ± 2° C.

Procedure

Poly(vinylferrocene) and PVFAN were electrodeposited in their oxidized forms as poly(vinylferricenium) perchlorate and poly(vinylferricenium acrylonitrile) perchlorate, respectively, onto the platinum disk electrode from stirred 0.1 *M* TBAP/CH_2Cl_2 solutions containing ca. 0.5 mg ml^{-1} of either PVF or PVFAN by maintaining the working electrode potential at 0.7 V (without *iR* compensation). To achieve more uniform film deposition, the working electrode was surrounded by a cylindrical platinum foil counter electrode. The quantity of material deposited was controlled by the electrolysis time: 30 s, ca. 7×10^{-8} mol Fc cm^{-2}; 5 min, ca. 3×10^{-7} mol Fc cm^{-2} (Fc = ferrocene group). The average thickness of the *dry* film was estimated from the charge consumed in completely reducing the film by stepping the potential from 0.9 to 0.2 V in acetonitrile solution as described previously, and the same caveats apply regarding the values obtained [5c].

Platinum electrodes thus coated were removed from the polymer-containing CH_2Cl_2 solution, shaken to remove any adhering solution and examined by cyclic voltammetry in MeCN solutions containing either 0.1 *M* TBAP or 0.1 *M* TEAPS, in which both redox forms of PVF and PVFAN were insoluble. The initial voltammograms were always identical to those obtained on subsequent scans, i.e. no "break-in period" was observed for either the PVF or the PVFAN films in the MeCN solutions.

RESULTS

Electrodeposited PVF films on platinum electrodes exhibited complex electrochemical behavior. Cyclic voltammograms observed for 0.14 μm PVF/Pt (dry thickness; 6.5×10^{-8} mol Fc cm^{-2}) in 0.1 *M* TBAP/MeCN at 0.01, 0.2 and 10 V s^{-1} are shown in Fig. 1. Even at the low scan rate of 0.01 V s^{-1} (Fig. 1A), a non-zero ΔE_p and a disparity in the half-widths and peak currents of the anodic and cathodic waves exists, suggesting significant differences in the nature and degree of interaction of the ferrocenes in the oxidized and reduced states. At higher scan rates, the waves gradually became more similar in appearance, ΔE_p increased and diffusional tailing was increasingly evident (Figs. 1B and 1C). These results were independent of the order in which the scan rate was varied.

Attempts at simulating the observed cyclic voltammetric behavior of the PVF films at 0.01, 0.2 and 10 V s^{-1} assuming that the structure of the film in 0.1 *M* TBAP/MeCN was homogeneous and that all the redox sites were characterized by the same value of E^0, were unsuccessful, even when interactions between redox centers were included. Improvements in the fit were obtained by including the following features: (a) the existence of several classes of ferrocene moieties in the film, each characterized by a different E^0 value; (b) the presence of attractive interactions between the ferrocenes; and (c) the interconversion of sites between two of these classes as a function of the redox state of the film. Details of the fitting process and values for the various parameters are given below. The model which was developed to explain the cyclic voltammetric behavior of PVF is first described.

(I) Models for the cyclic voltammetric behavior of multilayer films

The surface film is assumed to be electronically non-conductive. The model is shown in Fig. 2 and the electrode reaction is represented as

$$A + ne = B \qquad (1)$$

where A is the oxidized form of the polymer and B the reduced form. Electron transfer to the electroactive groups in the film proceeds in an outward direction from the electrode surface towards the film—solution interface. Direct electron transfer between the electrode and the film involves only those redox centers in the layer immediately adjacent to the electrode surface, (i.e. in box 1 in the simulation). Subsequent charge transfer to sites in layers further from the electrode surface (in boxes 2 through *JMAX*) is driven by the difference between the ratio of oxidized to reduced sites in the film and that required by the Nernst equation at the applied potential. The rate at which equilibrium is attained depends on the rate of transport of counter ions into or out the film and the rate of electron transfer between the electroactive groups. This latter process, which depends on such factors as the rate of achievement of the appropriate orientation of these goups, is related to the self-diffusion of the polymer chains [13]. The combined effect of electron transfer (or electron "hopping") between the electroactive groups on the polymer and counter ion movement is treated within the model as a diffusional process. When such pro-

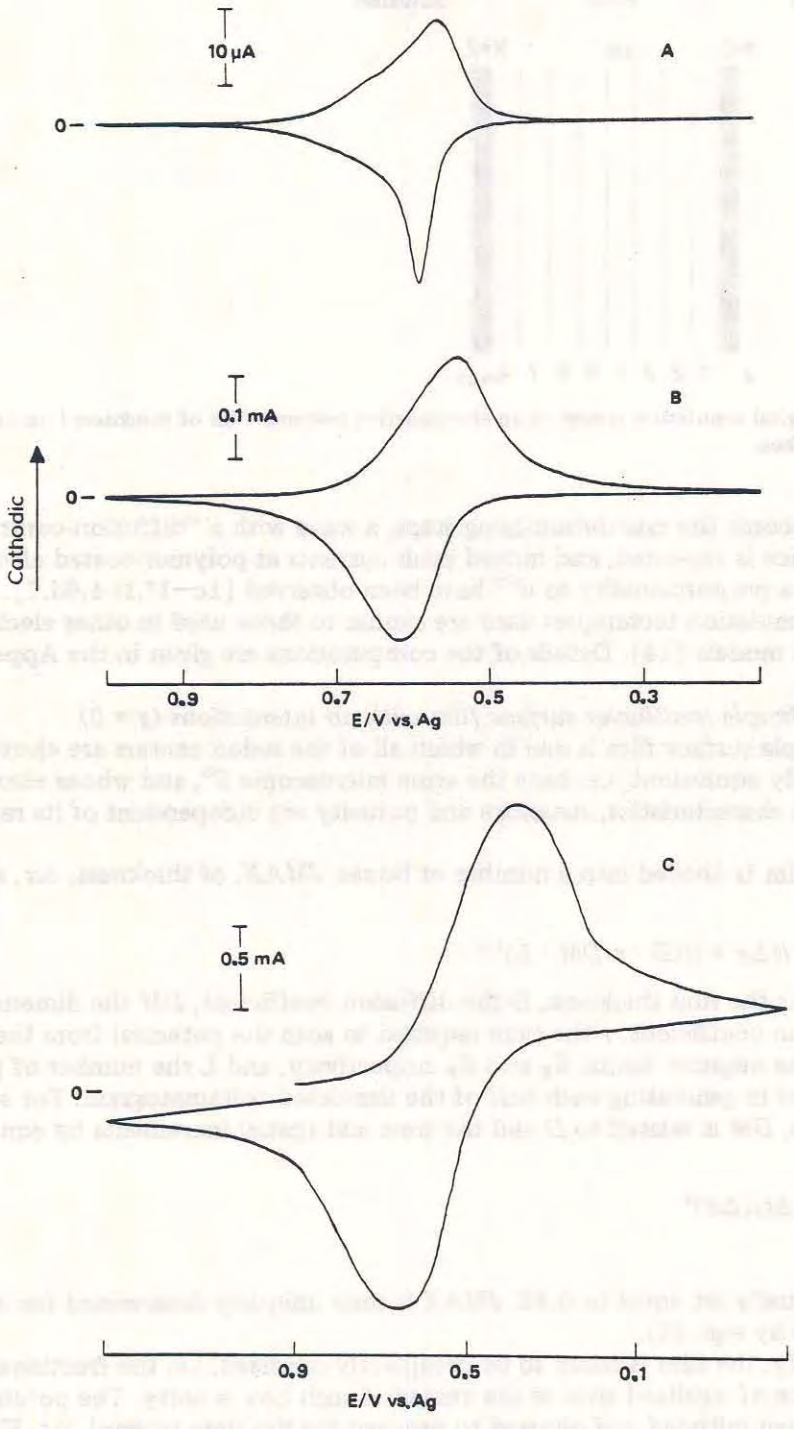

Fig. 1. Cyclic voltammograms for 0.14 μm PFV film (dry thickness; 6.5×10^{-8} mol Fc cm^{-2}) on a platinum electrode (area: 0.035 cm^2) in 0.1 *M* TBAP/MeCN. Scan rates: (a) 0.01 V s^{-1}; (b) 0.2 V s^{-1}; (C) 10 V s^{-1}.

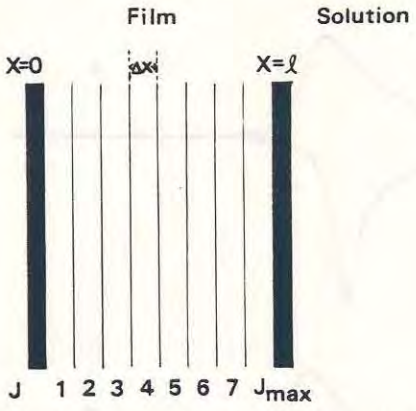

Fig. 2. Digital simulation model of an electroactive polymer film of thickness l on an electrode surface.

cesses become the rate-determining steps, a wave with a "diffusion-controlled" appearance is expected, and indeed peak currents at polymer-coated electrodes showing a proportionality to $v^{1/2}$ have been observed [1c—1f,1i,4,6d,7]. The digital simulation techniques used are similar to those used in other electrochemical models [14]. Details of the computations are given in the Appendix.

(I-1) Simple multilayer surface film with no interactions (g = 0)

A simple surface film is one in which all of the redox centers are electrochemically equivalent, i.e. have the same microscopic E^0, and whose electrochemical characteristics, structure and porosity are independent of its redox state.

The film is divided into a number of boxes, *JMAX*, of thickness, Δx, and area A,

$$JMAX = l/\Delta x = l/(D \cdot \tau/DM \cdot L)^{1/2} \quad (2)$$

where, l is the film thickness, D the diffusion coefficient, *DM* the dimensionless simulation coefficient, τ the time required to scan the potential from the positive to the negative limits, E_S and E_F respectively, and L the number of points calculated in generating each half of the simulated voltammogram. For solution reactants, *DM* is related to D and the time and spatial increments by eqn. (3) [14]:

$$DM = D\ \Delta t/(\Delta x)^2 \quad (3)$$

$$L = \tau/\Delta t \quad (4)$$

DM is usually set equal to 0.45. *JMAX* it then uniquely determined for each scan rate by eqn. (2).

Initially, the film is taken to be completely oxidized, i.e. the fractional concentration of oxidized sites at the center of each box is unity. The potential scan is then initiated and allowed to proceed for the time interval, Δt. Electron transfer between the electrode and the electroactive groups in box 1 alters the concentrations of the reduced and oxidized sites in box 1. The rate of this elec-

tron transfer is dependent on the overpotential and the simulation standard heterogeneous rate constant, *RKS*:

$$RKS = k^0\tau/L \qquad (5)$$

where k^0 is the real, standard heterogeneous electron transfer rate constant in s^{-1}. The simulation rate constants at a given potential, *RKF* and *RKB*, are given by eqns. (A4) and (A5). Charge transfer then occurs in boxes 2 through *JMAX* and the concentrations of the reduced and oxidized sites throughout the film are adjusted using the finite difference form of Fick's second law. The potential is then scanned for another time increment, Δt, and the process repeated until the entire scan is completed.

If the rate of charge transfer and diffusion through the film is fast compared to the scan rate so that the Nernst equation is satisfied by the entire film at every potential, the film behavior approaches that of a monolayer, i.e. *JMAX* = 1. At higher scan rates, diffusion within the bulk of the film may become rate limiting. The voltammetric waves then show diffusional tailing similar to that observed for dissolved reactants, but the current still eventually decays to zero because the diffusional situation is not semi-infinite. This case is readily distinguished from slow heterogeneous electron transfer because, in the latter case, the current rises more slowly but decays as exp(—t) [10a]. Moreoever, if diffusion within the film is rate determining, i_p will be linearly dependent on $v^{1/2}$ and, as long as k^0/v is greater than ca. 10^2 V^{-1}, ΔE_p will be equal to $59/n$ mV and scan-rate independent. However, if the hetereogeneous electron-transfer reaction were rate determining, i_p would be linearly dependent on v and ΔE_p would increase by $2.3RT/\alpha nF$ mV for each tenfold increase in the scan rate [10a]. At still higher scan rates, mixed control may be observed. The behavior for this case is thus the same as the familiar thin-layer cell behavior; however, the diffusion within the film may in fact represent internal electron-transfer limitations as well as actual mass transfer effects of the counter ions.

Simulated cyclic voltammograms demonstrating the electrochemical behavior of a simple surface film with no interactions are shown by the solid curves in Fig. 3. Although the simulations are carried out in terms of dimensionless parameters as described, they are represented here in terms of typical values of D, k^0, l, . . . to allow easier comparison to the experimental results. At 0.01 V s^{-1} (Fig. 3A), the waves exhibit all the characteristics expected for surface-confined reactants: symmetrical shape, $\Delta E_{1/2}$ = 90 mV, ΔE_p = 0 and equal peak currents ($i_{pa} = i_{pc}$). At 0.2 V s^{-1} (Fig. 3B), for the selected k^0 value the heterogeneous electron-transfer reaction is still rapid ($k^0/v = 10^3$), but tailing and a ΔE_p of 57 mV signal limitations in the rate of diffusion through the film. At 10 V s^{-1} (Fig. 3C), the electrode reaction is no longer nernstian ($k^0/v = 20$) as shown by the value ΔE_p = 250 mV; the shape of the individual waves resembles those for diffusing reactants.

(I-2) Simple multilayer surface film with interactions ($g \neq 0$)

Interactions between the electroactive groups in the film affect the half-widths, peak currents and peak potentials of the observed waves [10]. The effect of interactions (e.g. of the oxidized form, A) on the electrochemical behavior of the film can be incorporated into the model by modifying the

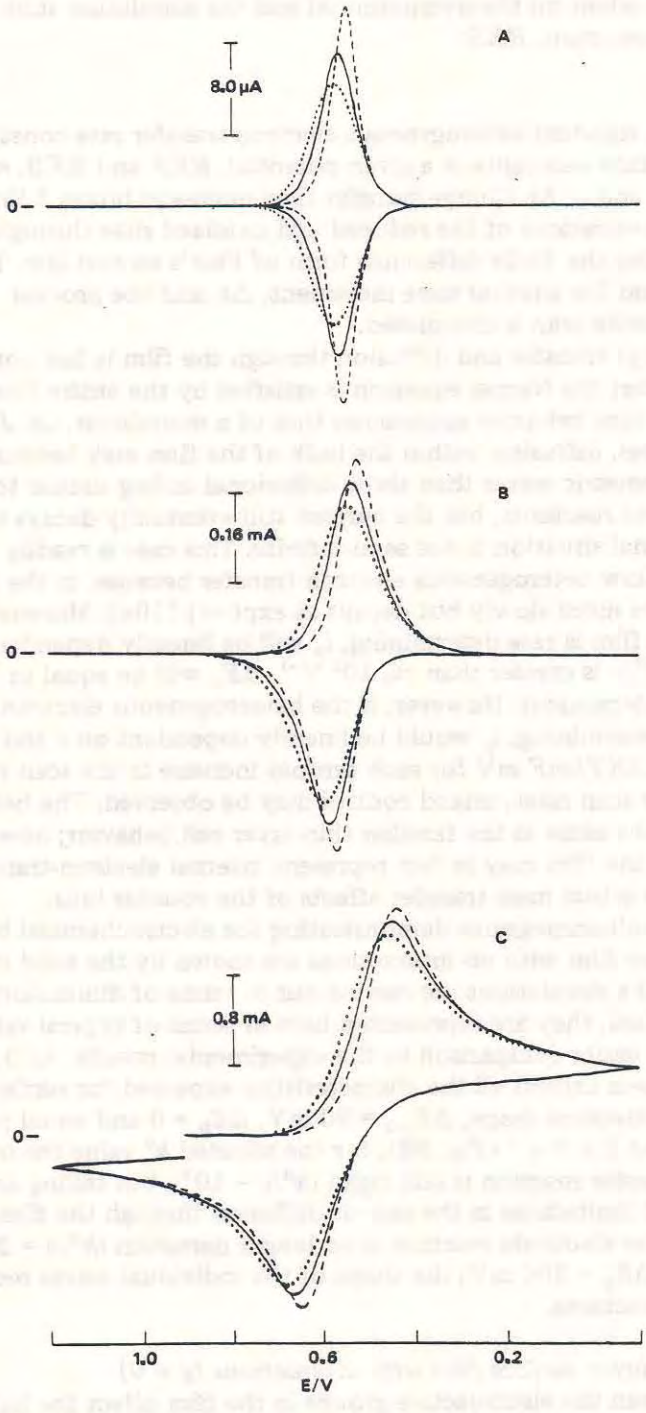

Fig. 3. Simulated cyclic voltammograms for a simple multilayer film on an electrode surface. E^0 = 0.56 V, k^0 = 200 s^{-1}, D = 2.7 × 10^{-10} cm^2 s^{-1}, Q = 220 μC, l = 0.14 μm. Scan rates: (A) 0.01 V s^{-1}; (B) 0.2 V s^{-1}; (C) 10 V s^{-1}. Interaction parameter: (———) AOX = 0; (- - - - - -) AOX = −1; (· · · · · ·), AOX = 1.

expressions for the forward (reduction) and reverse (oxidation) electrochemical rate constants (k_f and k_b) so that

$$k_f = k^0 \exp[-(\alpha nF/RT)(E - E^0)] \exp[\alpha\, g\, \theta_A] \quad (6)$$

$$k_b = k^0 \exp[(1-\alpha)(nF/RT)(E - E^0)] \exp[-(1-\alpha) g\, \theta_A] \quad (7)$$

where g is an interaction parameter and θ_A is the fractional coverage of the oxidized form at the electrode surface [10]. At equilibrium these equations produce the usual adsorption isotherm at the electrode surface. These equations in the digital simulation format are written:

$$RKF = RKS \exp[-(\alpha nF/RT)(E - E^0)] \exp[\alpha \cdot AOX \cdot FCA(1)] \quad (8)$$

$$RKB = RKS \exp[(1-\alpha)(nF/RT)(E - E^0)] \exp[-(1-\alpha) \cdot AOX \cdot FCA(1)] \quad (9)$$

where AOX is the simulation interaction parameter and is positive for repulsive interactions and negative for attractive interactions and $FCA(1)$ is the fractional concentration of oxidized sites in box 1 (at the electrode surface). In the model adopted here only interactions at the electrode surface are considered. In this case their effect is propagated throughout the film through the influence of surface processes on the subsequent fractional concentrations in the film. It is also possible that direct interactions occur between centers within the film; such effects can be incorporated into the model by a similar modification. Thus, attractive interactions between the oxidized centers enhances the rate of oxidation (formation of A) and decreases the rate of reduction. Consequently, both the anodic and cathodic waves exhibit larger peak currents and narrower half-widths than those in the absence of interactions, and they are shifted from E^0 towards more negative potentials. They are symmetric with $\Delta E_p = 0$. Simulated voltammograms with $AOX = -1$ are shown by the dashed lines in Fig. 3.

Repulsive interactions have the opposite effect on the observed cyclic voltammetric waves. Compared to the zero interaction case, the waves are broader, the peak currents are smaller and the direction of the peak potential shift is towards positive potentials. Simulated voltammograms with $AOX = 1$ are depicted by the dotted lines in Fig. 3. Parallel effects would be observed for interactions between the reduced centers.

The observed cyclic voltammogram reflects the net result of all the interactions in the film. For example, if the interactions between the oxidized and reduced sites were of the same type and magnitude, the observed waves would be indistinguishable from those for a film with no interactions.

(I-3) Multilayer surface film containing electrochemically non-equivalent redox sites — distribution independent of redox state of film

Although the observation of narrow waves unambiguously signals the presence of attractive interactions, broad waves can be caused by factors other than repulsive interactions. Broadening could also occur if all of the redox sites in the film were not characterized by the same value of E^0. For example, the existence of two types of sites may be signaled by the observation of shoulders on the waves.

The structure of polymers adsorbed on solid surfaces, e.g. silica is not homogeneous. There is experimental evidence of a higher density of polymer seg-

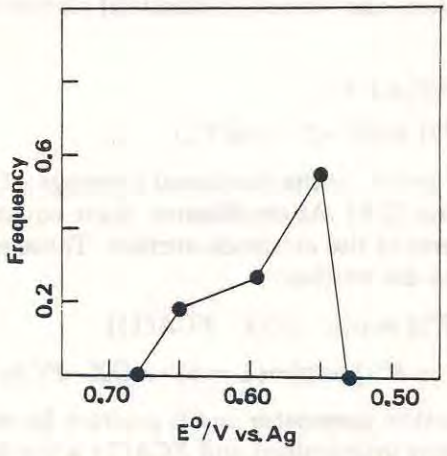

Fig. 4. Fractional distribution of the different classes of redox sites in an adsorbed polymer film. Class limits: 0.680—0.620 V, midpoint = 0.650 V, fraction = 0.18; 0.619—0.570 V, midpoint = 0.595 V, fraction = 0.27; 0.569—0.530 V, midpoint = 0.550 V, fraction = 0.55.

ments at an adsorbing surface than in the layers further from the surface [15]. The distribution of segments as a function of distance from the interface for a single, infinitely long polymer chain adsorbed at the interface has been treated by Hoeve [16]. The density was shown to drop suddenly at a small distance from the interface and then to decrease exponentially beyond this distance for long chains. Consequently, it seem reasonable to expect the structure of a multilayer polymer film adsorbed on an electrode surface to be inhomogeneous. In such a film, the chemical environments of the individual redox centers may well be sufficiently different to alter their reduction potentials.

The presence of electrochemically non-equivalent sites in the film is incorporated into the model by dividing the electroactive groups into several classes with different E^0 values which characterize the behavior of the film. The number of different classes and the fraction of sites in each class is chosen to yield the best fit to the data and the initial conditions are appropriately modified; e.g. for three classes (Fig. 4):

$$FCA1(J) = f_1; \qquad FCA2(J) = f_2; \qquad FCA3(J) = 1 - (f_1 + f_2)$$

$$FCB1(J) = 0; \qquad FCB2(J) = 0; \qquad FCB3(J) = 0$$

where, f_1 and f_2 are the values for the fractional concentrations of oxidized sites in classes 1 and 2 respectively, and $FCAn(J)$ and $FCBn(J)$ are the fractional concentrations of oxidized and reduced sites respectively, of class n in the Jth box. In the simplest case, transformation between classes does not occur and each is assumed to behave independently, i.e. there is no interclass electron transfer. Values of E_n^0, k_n^0 and D_n are chosen to fit the data over the entire range of scan rates. The value of DM for one of the classes may be chosen arbitrarily. However, as $JMAX$ must be the same for each class of redox sites, the over values of DM must satisfy the equation:

$$DM1/D_1 = DM2/D_2 = DM3/D_3 \qquad (10)$$

Simulation of the cyclic voltammograms then follows the procedure outlined above for the simple multilayer surface film except that now there are three sites to be considered. Interactions for any or all of the classes may be introduced as described above.

(I-4) Multilayer surface film containing electrochemically non-equivalent redox sites — distribution a function of redox state of film

A change in the degree of swelling of the polymer film may well accompany a change in its redox state, especially if the film is uncharged in one of its redox states. Such a change, as well as other structural modifications during the course of the redox reaction, can be incorporate into the model as transformations between the different classes during the scan. These changes will cause a non-zero, scan-rate-independent ΔE_p over a range of scan rates which are slow compared to the rate of interconversion. If in the example described in the preceding section this redistribution of sites involves only classes 1 and 2, it may be represented by the following scheme:

Scheme 1

$$\begin{array}{ccc} \mathrm{A1} + e^- & \overset{E_1^0}{\rightleftharpoons} & \mathrm{B1} \\ {\scriptstyle K_A}\ \uparrow\downarrow & & \uparrow\downarrow\ {\scriptstyle K_B} \\ \mathrm{A2} + e^- & \overset{E_2^0}{\rightleftharpoons} & \mathrm{B2} \end{array}$$

At equilibrium:

$$FCA1(J)/FCA2(J) = K_A \tag{11}$$

$$FCB2(J)/FCB1(J) = K_B \tag{12}$$

where K_A and K_B are equilibrium constants. Here, K_A is fixed by the initial conditions and the value of K_B must be consistent with the values of E_1^0 and E_2^0;

$$E_1^0 = E_2^0 - 0.059 \log(K_A K_B) \tag{13}$$

First-order rate constants k_A and k_B, for the conversion of A2 to A1 and B1 to B2 respectively, are chosen. The corresponding simulation rate constants are given by

$$XKA = (k_A/v)(E_S - E_F)/L \tag{14}$$

$$XKB = (k_B/v)(E_S - E_F)/L \tag{15}$$

The reverse rate constants, $XKAR$ and $XKBR$, are XKA/K_A and XKB/K_B respectively. Correction for this redistribution of sites in classes 1 and 2 within a given time increment is made in the simulation after the diffusional processes.

Physically, one may also regard this redistribution of sites in classes 1 and 2 as a consequence of electron transfer between classes:

$$\mathrm{B1} + \mathrm{A2} \rightarrow \mathrm{A1} + \mathrm{B2} \tag{16}$$

This interpretation requires that $k_A = k_B$ and $K_A = K_B$. It is also possible that the oxidation or reduction of a surface film may be accompanied by complete rearrangement of the film structure such that the reactions in the proposed

scheme are irreversible, i.e. only Al is present in the oxidized film and B2 in the reduced film. Behavior suggestive of such a process has been observed for TTF (tetrathiafulvalane) films in aqueous solutions containing Cl^-, Br^- or I^- ions [17]; for TCNQ (tetracyanoquinodimethane) films in aqueous solutions containing Na^+ of K^+ ions [17]; and for TTF—TCNQ electrodes in aqueous 1 *M* KBr [17a,18].

(II) Cyclic voltammetric behavior of electrodeposited PVF films on Pt

We now describe experimental results for the cyclic voltammetry of electrodeposited PVF films on platinum electrodes. Both TBAP and TEAPTS were used as supporting electrolytes in order to study the effect of the counter ion size on the redox behavior of the polymer film. Data were obtained at 14 different scan rates from 0.002 to 50 V s^{-1}. In a study of a given film the scan rates were applied in a random manner to avoid time-dependent effects arising from changes in the chemical properties of the film caused by repeated cycling. (no such changes were actually observed with these electrodes.) To determine whether some of the film was being lost during the course of the experiment, a voltammogram was run at a reference scan rate (0.1 V s^{-1}) after every third scan. Over a period of 1.5 h, the integrated area under the anodic and cathodic waves at 0.1 V s^{-1} typically decreased by ca. 10%.

Vinylferrocene is known to form an alternating copolymer with acrylonitrile [12] and a similar study was also made of the electrochemical behavior of electrodeposited PVFAN films in order to assesss the effect of increasing the spacing between the electroactive ferrocene groups on the rate of charge transfer in the film.

(II-1) Poly(vinylferrocene)

Typical cyclic voltammograms at 0.01, 0.2 and 10 V s^{-1} for 0.14 μm PVF/Pt (dry thickness; 6.5×10^{-8} mol Fc cm^{-2}) in 0.1 *M* TBAP/MeCN are shown in Fig. 1 and data at each different scan rate are given in Table 1. Below 0.1 V s^{-1}, the shapes of the cathodic and anodic waves were markedly different. At scan rates of 0.01 V s^{-1} or less, i_{pa}/i_{pc} was 1.6, the half-width of the anodic wave was 40 mV compared to 100 mV for the cathodic wave and ΔE_p was 20 mV independent of the scan rate. As the scan rate was increased from 0.01 to 0.2 V s^{-1}, i_{pa}/i_{pc} gradually approached unity, the anodic wave broadened and ΔE_p increased to 75 mV. At 0.1 V s^{-1}, ΔE_p was 58 mV. Below 0.2 V s^{-1}, both waves exhibited a distinct shoulder at ~0.65 V.

The shape of the anodic wave depended only on the rate of oxidation of the film. The narrow anodic wave was observed when the PVF film was reduced at 0.2 V s^{-1} and reoxidized at 0.01 V s^{-1}, but not when it was reduced at 0.01 V s^{-1} and reoxidized at 0.2 V s^{-1}.

Above 0.2 V s^{-1}, the cathodic and anodic waves were similar in appearance and ΔE_p increased to 400 mV at 50 V s^{-1}. Diffusional tailing for both waves was evident at 0.2 V s^{-1}. Above 1 V s^{-1}, the shape of the waves resembled those for dissolved reactants. Between 10 V s^{-1} (Fig. 1C) and 50 V s^{-1}, a shoulder was evident on the reduction wave at potentials negative of E_{pc} which was matched by a shoulder on the oxidation wave at potential positive of E_{pa}.

TABLE 1

Cyclic voltammetric data for poly(vinylferrocene)-coated electrodes in acetonitrile solutions

Scan rate v/V s^{-1}	$i_{pc}\, v^{-1}$/ mA s V^{-1}	$i_{pa}\, v^{-1}$/ mA s V^{-1}	$i_{pc}\, v^{-1/2}$/ mA s$^{1/2}$ V$^{-1/2}$	$i_{pa}\, v^{-1/2}$/ mA s$^{1/2}$ V$^{-1/2}$
A. 0.14 μm (dry thickness) PVF/Pt in 0.1 *M* TBAP/MeCN				
0.002	1.40	2.19	0.063	0.098
0.005	1.37	2.16	0.097	0.15
0.01	1.32	2.12	0.13	0.21
0.02	1.25	1.92	0.18	0.27
0.05	1.15	1.59	0.26	0.36
0.1	1.03	1.28	0.32	0.40
0.2	0.90	0.96	0.40	0.43
0.5	0.68	0.66	0.48	0.47
1.0	0.52	0.50	0.52	0.50
2.0	0.37	0.35	0.53	0.49
5.0	0.21	0.21	0.48	0.48
10.0	0.16	0.16	0.51	0.51
20.0	0.11	0.11	0.48	0.48
50.0	0.068	0.068	0.48	0.48
B. 0.18 μm (dry thickness) PVF/Pt in 0.1 *M* TEAPTS/MeCN				
0.002	2.74	9.85	0.12	0.44
0.005	2.82	8.38	0.20	0.59
0.01	2.77	7.16	0.28	0.72
0.02	2.66	5.02	0.38	0.71
0.05	2.41	3.35	0.54	0.75
0.1	2.22	2.66	0.70	0.84
0.2	1.71	1.48	0.76	0.66
0.5	1.38	1.11	0.97	0.78
1.0	0.96	0.74	0.96	0.74
2.0	0.66	0.48	0.94	0.68
5.0	0.38	0.29	0.86	0.64
10.0	0.27	0.22	0.86	0.70
20.0	0.20	0.16	0.90	0.73
50.0	0.13	0.099	0.92	0.70
C. 0.14 μm (dry thickness) PVFAN/Pt in 0.1 *M* TBAP/MeCN				
0.002	0.86	0.92	0.039	0.041
0.005	0.98	1.02	0.070	0.072
0.01	1.02	1.08	0.10	0.11
0.02	0.94	0.94	0.13	0.13
0.05	0.88	0.90	0.20	0.20
0.10	0.87	0.75	0.28	0.24
0.20	0.52	0.41	0.23	0.18
0.5	0.61	0.39	0.43	0.27
1.0	0.41	0.28	0.41	0.28
2.0	0.32	0.20	0.46	0.28
5.0	0.19	0.11	0.42	0.26
10.0	0.18	0.15	0.56	0.47
20.0	0.093	0.064	0.42	0.29
50.0	0.057	0.040	0.40	0.28
D. 0.17 μm (dry thickness) PVFAN/Pt in 0.1 *M* TEAPTS/MeCN				
0.002	1.97	2.08	0.088	0.093
0.005	1.97	2.24	0.14	0.16
0.01	1.96	2.29	0.20	0.23

Table 1 (continued)

Scan rate v/V s^{-1}	$i_{pc}\, v^{-1}$/ mA s V^{-1}	$i_{pa}\, v^{-1}$/ mA s V^{-1}	$i_{pc}\, v^{-1/2}$/ mA $s^{1/2}$ $V^{-1/2}$	$i_{pa}\, v^{-1/2}$/ mA $s^{1/2}$ $V^{-1/2}$
0.01	1.72	1.74	0.24	0.25
0.05	1.41	1.16	0.32	0.26
0.1	1.26	1.04	0.40	0.33
0.2	0.68	0.37	0.31	0.16
0.5	0.54	0.34	0.38	0.24
1.0	0.34	0.20	0.34	0.20
2.0	0.23	0.14	0.32	0.20
5.0	0.13	0.089	0.30	0.20
10.0	0.11	0.093	0.36	0.29
50.0	0.042	0.030	0.30	0.21

The peak currents were linearly dependent on the scan rate between 0.002 and 0.01 V s^{-1} and were linearly dependent on the square root of the scan rate between 0.5 and 50 V s^{-1} (Table 1). The change consumed in reducing or oxidizing the PVF film decreased as the scan rate was increased, indicating that increasingly fewer ferrocenes were able to participate in the electron-transfer reaction as the time for the reaction was shortened. This result is consistent with the fact that at the faster scan rates the current did not decay to zero before the switching potential was reached.

Cyclic voltammograms for 0.18 μm PVF/Pt (dry thickness 8.4×10^{-8} mol Fc cm^{-2}) in 0.1 *M* TEAPTS/MeCN at 0.002, 0.01, 0.2 and 10 V s^{-1} are shown in Fig. 5. The cathodic behavior of PVF in the presence of PTS^- was somewhat different from that observed in perchlorate at 0.01 V s^{-1} or less (Figs. 5A and 5B). In PTS^- the reduction wave was narrower and more symmetrical and its peak potential was 30 mV more negative than in ClO_4^- (0.52 vs. 0.55 V). Although E_{pc} shifted negative more rapidly in PTS^- as the scan rate was increased, tailing was apparent only at scan rates of 1 V s^{-1} or higher. The peak current was proportional to v below 0.05 V s^{-1}, and to $v^{1/2}$ between 1 and 50 V s^{-1}. (Table 1).

The oxidation behavior of PVF was strongly affected by the change in the counter ion from perchlorate to PTS^-. In PTS^-, the anodic wave was characterized by a shoulder at ~0.53 V followed by a sharp spike at 0.55 V. As in perchlorate, the appearance of the sharp anodic spike was dependent only on the rate of the anodic sweep. Even when the scan direction was reversed on the descending branch of the cathodic peak, the spike was still observed provided $v < 0.05$ V s^{-1}. As the scan rate was increased, both anodic waves shifted to more positive potentials and the spike gradually became broader until the two waves merged at 0.5 V s^{-1}. The peak current was proportional to $v^{1/2}$ between 1 and 50 V s^{-1}. Above 2 V s^{-1}, the shapes of the anodic and cathodic waves were similar to those for dissolved reactants. The fraction of the film electrolyzed decreased as the scan rate was increased.

(II-2) Poly(vinylferrocene acrylonitrile)

Cyclic voltammograms for 0.14 μm PVFAN/Pt (dry thickness 5.3×10^{-8} mol

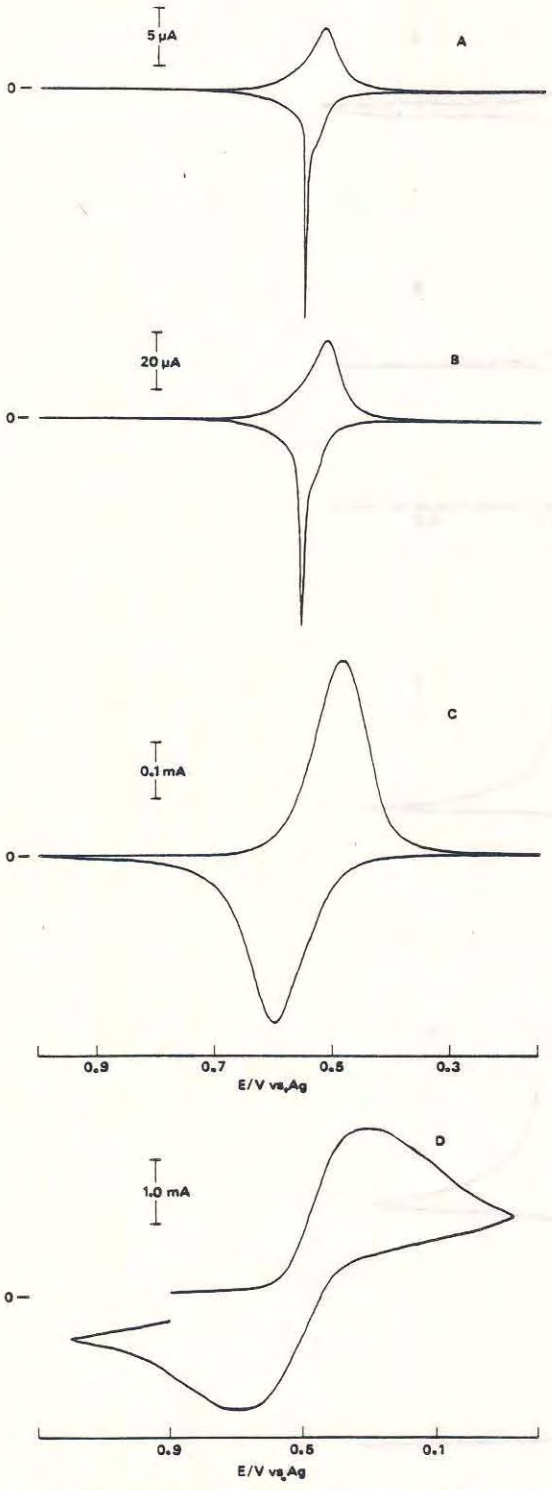

Fig. 5. Cyclic voltammograms for 0.18 μm PVF film (dry thickness; 8.4×10^{-8} mol Fc cm^{-2}) on a platinum electrode (area: 0.035 cm^2) in 0.1 *M* TEAPTS/MeCN. Scan rates: (A) 0.002 V s^{-1}; (B) 0.01 V s^{-1}; (C) 0.2 V s^{-1}; (D) 10 V s^{-1}.

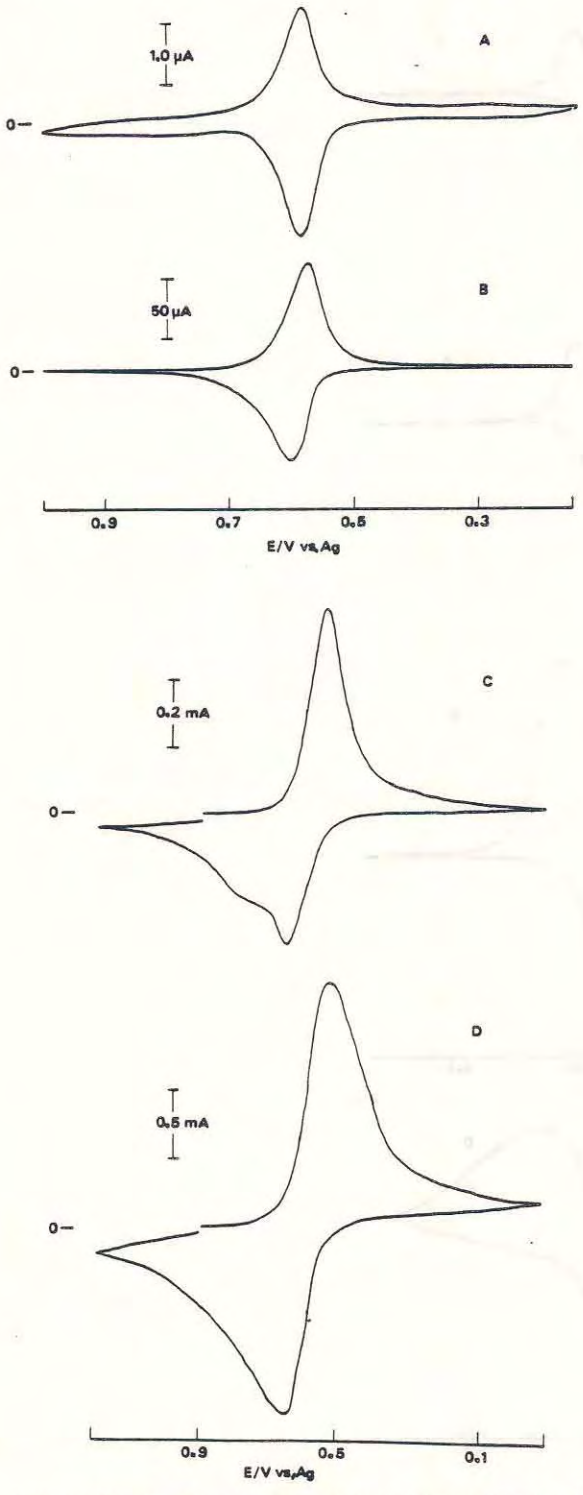

Fig. 6. Cyclic voltammograms for 0.14 μm PVFAN film (dry thickness; 5.3×10^{-8} mol Fc cm^{-2}) on a platinum electrode (area: 0.035 cm^2) in 0.1 *M* TBAP/MeCN. Scan rates: (A) 0.002 V s^{-1}; (B) 0.1 V s^{-1}; (C) 2 V s^{-1}; (D) 10 V s^{-1}.

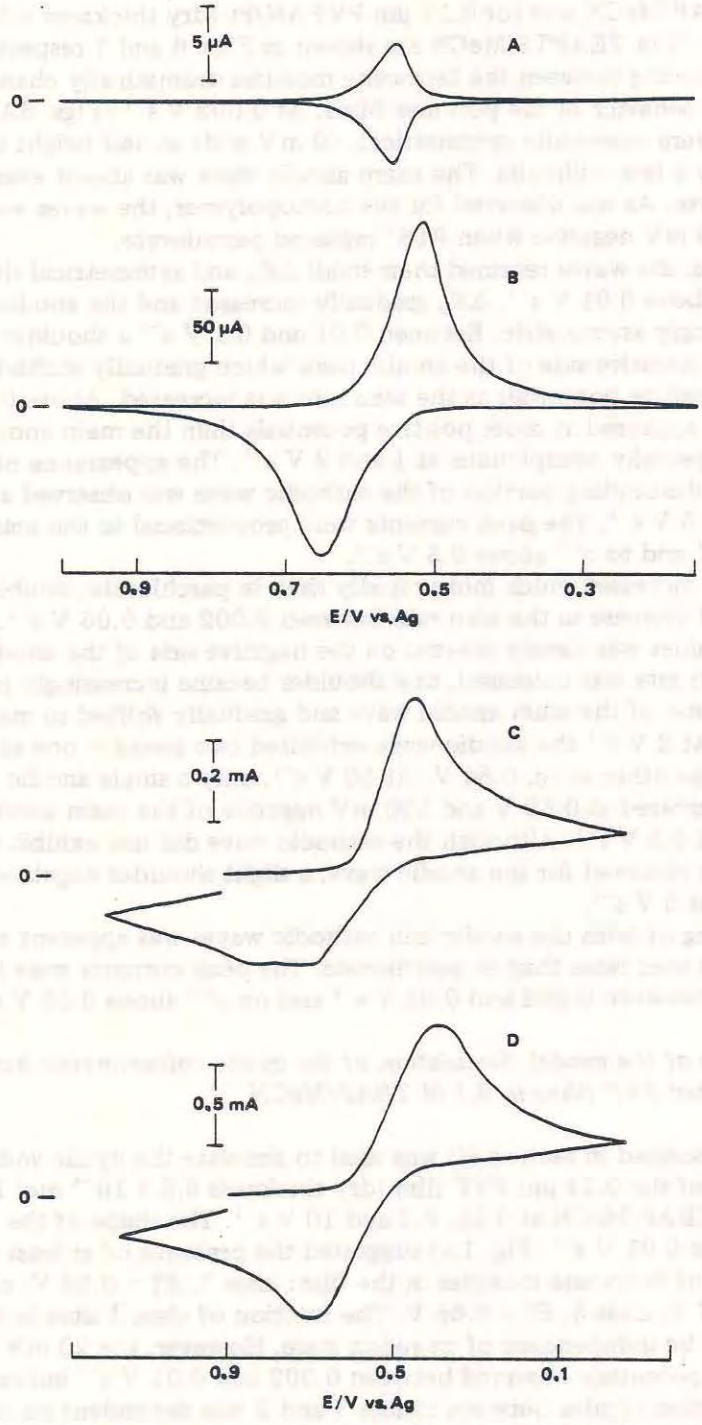

Fig. 7. Cyclic voltammograms for 0.17 μm PVFAN film (dry thickness; 6.5×10^{-8} mol Fc cm^{-2}) on a platinum electrode (area: 0.035 cm^2) in 0.1 *M* TEAPTS/MeCN. Scan rates: (A) 0.002 V s^{-1}; (B) 0.1 V s^{-1}; (C) 2 V s^{-1}; (D) 10 V s^{-1}.

Fc cm^{-2}) in TBAP/MeCN and for 0.17 μm PVFAN/Pt (dry thickness 6.5 × 10^{-8} mol Fc cm^{-2}) in TEAPTS/MeCN are shown in Figs. 6 and 7 respectively. The increased spacing between the ferrocene moieties dramatically changed the electrochemical behavior of the polymer films. At 0.002 V s^{-1} (Figs. 6A and 7A) the waves were essentially symmetrical, 60 mV wide at half height and separate by only a few millivolts. The sharp anodic wave was absent even with a PTS^- electrolyte. As was observed for the homopolymer, the waves were shifted about 30 mV negative when PTS^- replaced perchlorate.

In perchlorate, the waves retained their small ΔE_p and symmetrical shape up to 0.01 V s^{-1}. Above 0.01 V s^{-1}, ΔE_p gradually increased and the anodic wave became increasingly asymmetric. Between 0.01 and 0.1 V s^{-1} a shoulder was apparent on the negative side of the anodic peak which gradually shifted towards more positive potentials as the scan rate was increased. Above 0.1 V s^{-1} the shoulder appeared at more positive potentials than the main anodic peak and was especially conspicuous at 1 and 2 V s^{-1}. The appearance of a shoulder on the descending portion of the cathodic wave was observed at scan rates faster than 5 V s^{-1}. The peak currents were proportional to the scan rate below 0.05 V s^{-1} and to $v^{1/2}$ above 0.5 V s^{-1}.

In PTS^-, ΔE_p increased much more rapidly than in perchlorate, doubling for each twofold increase in the scan rate between 0.002 and 0.05 V s^{-1}. At 0.1 V s^{-1}, a shoulder was clearly present on the negative side of the anodic peak. As the scan rate was increased, this shoulder became increasingly prominent at the expense of the main anodic wave and gradually shifted to more positive potentials. At 2 V s^{-1} the anodic wave exhibited two peaks — one at ca. 0.68 V s^{-1} and the other at ca. 0.84 V. At 10 V s^{-1}, only a single anodic wave was observed, centered at 0.69 V and 130 mV *negative* of the main anodic wave observed at 0.5 V s^{-1}. Although the cathodic wave did not exhibit the obvious splitting observed for the anodic wave, a slight shoulder negative of E_{pc} was discernible at 5 V s^{-1}.

In PTS^-, tailing of both the anodic and cathodic waves was apparent at significantly slower scan rates than in perchlorate. The peak currents were linearly dependent on v between 0.002 and 0.01 V s^{-1} and on $v^{1/2}$ above 0.05 V s^{-1}.

(III) Application of the model. Simulation of the cyclic voltammetric behavior of electrodeposited PVF films in 0.1 M TBAP/MeCN

The model described in section (*I*) was used to simulate the cyclic voltammetric behavior of the 0.14 μm PVF film (dry thickness 6.5 × 10^{-8} mol FC cm^{-2}) in 0.1 *M* TBAP/MeCN at 0.01, 0.2 and 10 V s^{-1}. The shape of the voltammogram at 0.01 V s^{-1} (Fig. 1A) suggested the presence of at least three different classes of ferrocene moieties in the film: class 1, $E_1^0 \sim 0.55$ V; class 2, $0.65 > E_2^0 > 0.57$ V; class 3, $E_3^0 \sim 0.65$ V. The fraction of class 3 sites in the film appeared to be independent of its redox state. However, the 20 mV separation in the peak potentials observed between 0.002 and 0.01 V s^{-1} indicated that the distribution of sites between classes 1 and 2 was dependent on the oxidation state of the film. The narrowness of the anodic wave signaled the presence of attractive interactions between the sites in class 2. As these interactions shift the peak potential in a negative direction, E^0's for these sites must

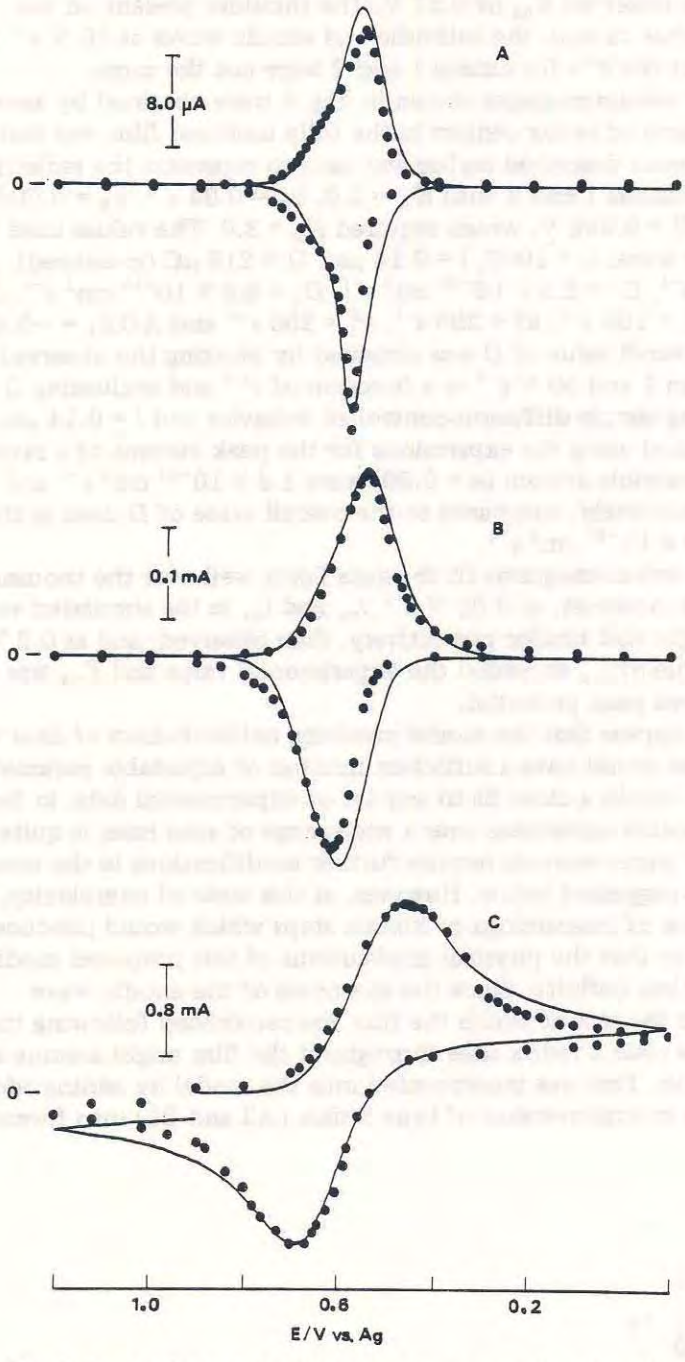

Fig. 8. Comparison of simulated and experimental cyclic voltammograms for 0.14 μm (dry thickness) PVF/Pt in 0.1 *M* TBAP/MeCN. Scan rates: (A) 0.01 V s^{-1}; (B) 0.2 V s^{-1}; (C) 10 V s^{-1}. (———) Simulated voltammograms assuming the initial distribution of redox sites shown in Fig. 4 and E_1^0 = 0.550 V, E_2^0 = 0.595 V, E_3^0 = 0.650 V, k_1^0 = 100 s^{-1}, k_2^0 = 200 s^{-1}, k_3^0 = 250 s^{-1}, $D_1 = 2.0 \times 10^{-10}$ cm^2 s^{-1}, $D_2 = 2.8 \times 10^{-10}$ cm^2 s^{-1}, $D_3 = 2.8 \times 10^{-10}$ cm^2 s^{-1}, $DM3$ = 0.45, AOX_2 = −2.40, Q = 219 μC (measured), l = 0.14 μm, L = 1000, K_A = 2.0, k_A = 0.04 s^{-1} and k_B = 0.008 s^{-1}; (●) experimental point obtained by digitizing the voltammograms shown in Fig. 1.

be positive of the observed E_{pa} of 0.57 V. The shoulder present on the descending branches of both the cathodic and anodic waves at 10 V s^{-1} (Fig. 1C) indicated that the k^0's for classes 1 and 2 were not the same.

The simulated voltammograms shown in Fig. 8 were obtained by assuming that the distribution of redox centers in the fully oxidized film was that shown in Fig. 4. The scheme described earlier was used to represent the redistribution of sites between classes 1 and 2 with $K_A = 2.0$, $k_A = 0.04$ s^{-1}, $k_B = 0.008$ s^{-1}, $E_1^0 = 0.550$ and $E_2^0 = 0.595$ V, which required $K_B = 3.0$. The values used for the other parameters were: $L = 1000$, $l = 0.14$ μm, $Q = 219$ μC (measured), $D_1 = 2.0 \times 10^{-10}$ cm^2 s^{-1}, $D_2 = 2.8 \times 10^{-10}$ cm^2 s^{-1}, $D_3 = 5.8 \times 10^{-10}$ cm^2 s^{-1}, $DM3 = 0.45$, $\alpha = 0.50$, $k_1^0 = 100$ s^{-1}, $k_2^0 = 200$ s^{-1}, $k_3^0 = 250$ s^{-1} and $AOX_2 = -2.40$. An estimate of the overall value of D was obtained by plotting the observed i_p's at scan rates between 1 and 50 V s^{-1} as a function of $v^{1/2}$ and evaluating D from the slope assuming simple diffusion-controlled behavior and $l = 0.14$ μm. The values of D obtained using the expressions for the peak current of a reversible and a totally irreversible system ($\alpha = 0.50$) were 1.3×10^{-10} cm^2 s^{-1} and 4.1×10^{-10} cm^2 s^{-1} respectively, compared to the overall value of D used in the simulation of 2.9×10^{-10} cm^2 s^{-1}.

The simulated voltammograms fit the data fairly well over the thousandfold range of scan rate; however, at 0.01 V s^{-1}, i_{pc} and i_{pa} in the simulated voltammogram were larger and smaller respectively, than observed; and at 0.2 V s^{-1} the calculated value of i_{pa} exceeded the experimental value and E_{pa} was negative of the observed peak potential.

While it might appear that the model involving redistribution of sites with different E^0 values would have a sufficient number of adjustable parameters and flexibility to obtain a close fit to any set of experimental data, in fact even obtaining a reasonable agreement over a wide range of scan rates is quite difficult. Any further improvements require further modifications in the model. One possibility is suggested below. However, at this state of complexity, there may be other types of interactions or kinetic steps which would produce equally good fits so that the physical implications of this proposed modification are probably less definite. Since the sharpness of the anodic wave depended only on the rate at which the film was reoxidized following the cathodic scan, the class 2 redox sites throughout the film might assume a more ordered orientation. This was incorporated into the model by adding additional rate constants for interconversion of type 2 sites (A2 and B2) into forms AX and BX:

Scheme 2

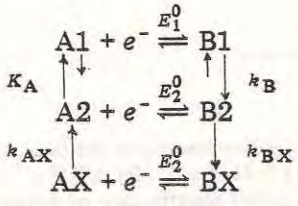

where AX and BX are the oxidized and reduced sites, respectively, in class 2 which have been reoriented, and k_{AX} and k_{BX} are first-order rate constants for

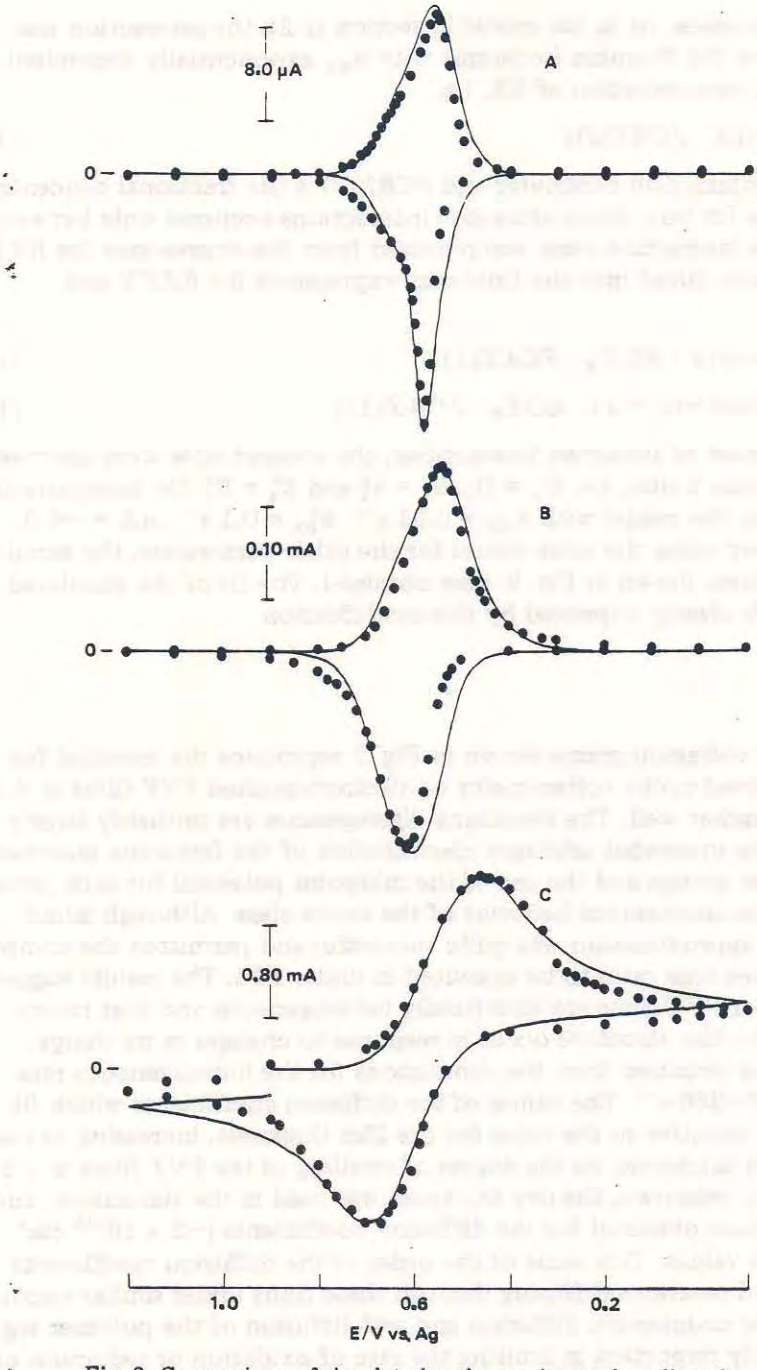

Fig. 9. Comparison of simulated and experimental cyclic voltammograms for 0.14 μm (dry thickness) PVF/Pt in 0.1 *M* TBAP/MeCN. Scan rates: (A) 0.01 V s^{-1}; (B) 0.2 V s^{-1}; (C) 10 V s^{-1}. (———) Simulated voltammograms using same values for each of the parameters as for Fig. 8 except that now attractive interactions arise from a slow ordering process which occurs during the oxidation of the film (see text); (●) experimental points obtained by digitizing the voltammograms shown in Fig. 1.

the indicated processes. As in the model in section (*I-2*), the interaction was assumed to follow the Frumkin isotherms with k_{BX} exponentially dependent on the fractional concentration of BX, i.e.

$$k_{BX} = k^0_{BX} \exp(-AX \cdot FCBX(J)) \quad (17)$$

where AX is an interaction parameter and $FCBX(J)$ is the fractional concentration of BX in the Jth box. Since attractive interactions occurred only between ordered sites, the interaction term was removed from the expressions for $RKF2$ and $RKB2$ and introduced into the following expressions for $RKFX$ and $RKBX$,

$$RKFX = RKF2 \exp[\alpha \cdot AOX_X \cdot FCAX(1)] \quad (18)$$

$$RKBX = RKB2 \exp[-(1-\alpha) \cdot AOX_X \cdot FCAX(1)] \quad (19)$$

Except for the onset of attractive interactions, the ordered sites were assumed to be similar to class 2 sites, i.e. $D_x = D_2$, $k^0_x = k^0_2$ and $E^0_x = E^0_2$. On incorporating these changes into the model with $k_{AX} = 0.01\ s^{-1}$. $k^0_{BX} = 0.1\ s^{-1}$, $AX = -6.0$, $AOX_x = -2.40$ and using the same values for the other parameters, the simulated voltammograms shown in Fig. 9 were obtained. The fit of the simulated voltammograms is clearly improved by this modification.

DISCUSSION

The simulated voltammograms shown in Fig. 9 reproduce the essential features of the observed cyclic voltammetry of electrodeposited PVF films in 0.1 *M* TBAP/MeCN rather well. The remaining discrepancies are probably largely attributable to the somewhat arbitrary classification of the ferrocene moieties into three discrete groups and the use of the midpoint potential for each group to describe the electrochemical behavior of the entire class. Although admittedly crude, this approximation was quite successful and permitted the computations for all three scan rates to be executed in under 10 s. The results suggest that the multilayer PVF films are structurally heterogeneous and that reversible changes in the film structure occur in response to changes in its charge density. The value obtained from the simulations for the heterogeneous rate constants are 100—250 s^{-1}. The values of the diffusion coefficients which fit the data are very sensitive to the value for the film thickness, increasing as the square of the film thickness. As the degree of swelling of the PVF films in 0.1 *M* TBAP/MeCN is unknown, the dry thickness was used in the simulation; consequently, the values obtained for the diffusion coefficients ($\sim 2 \times 10^{-10}$ cm^2 s^{-1}) are minimum values. This value of the order of the diffusion coefficients for small dissolved reactants diffusing through these films under similar conditions [5c], so that counter-ion diffusion and self-diffusion of the polymer segments are probably important in limiting the rate of oxidation or reduction of the film.

Changes in the counter ion and in the spacing between the ferrocene moieties had a marked effect on the cyclic voltammetric behavior of the film. The extremely narrow anodic wave observed for PVF in 0.1 *M* TEAPTS/MeCN (half-width: 10 mV at 0.002 V s^{-1}) indicates that a much higher degree of

order was achieved in the presence of PTS^- compared to perchlorate. Similar effects have been found with electrodes fabricated from the highly ordered, organic metal TTF—TCNQ, which exhibit very narrow waves in aqueous 1 *M* KBr [17,18]. The smaller apparent heterogeneous rate constants in PTS^- compared to perchlorate, was indicated by the more rapid increase in ΔE_p, unaccompanied by any evidence of tailing. The decrease in the apparent rate of the electrode reaction is probably due to stronger ion-pairing with PTS^-. The observed shift in E_{pc} to more negative potentials with PTS^- supports this interpretation.

In PVFAN the ferrocenes are separated by an additional two carbon atoms. The symmetrical shapes of the waves for the electrodeposited PVFAN films in both perchlorate and PTS^- suggest that the charge density in the oxidized PVFAN films is much less than in oxidized PVF films so that little change in the structure of PVFAN films accompanies changes in the redox state. The presence of weakly attractive interactions between the redox sites is indicated by the obserbed 60 mV half-width at slow scan rates; however, the increased spacing between the ferrocenes apparently prevents the occurence of the ordering process observed for PVF films. The obvious splitting of the anodic wave for the PVFAN films in both perchlorate and PTS^- indicates that these films are also structurally heterogeneous. The apparent heterogeneous electron-transfer rate constant for PVF is lower in PTS^- than in perchlorate and the peak potentials are shifted some 30 mV negative, again, perhaps, as a result of ion-pairing between Fc^+ and PTS^-.

CONCLUSIONS

A model useful in interpreting current—potential curves obtained with polymer films has been presented. The main features of this model include the existence of different types of oxidized (and reduced) sites in the film which reflect different environments within the film. Interconversion of these sites, as well as interactions between the sites, must be included. The rate of the electrochemical reaction depends upon the rate of interconversion, as well as the rates of heterogeneous electron transfer between substrate and film, intrafilm electron transfer and diffusion of counter ions within the film. The electrochemical behavior of polymer films depends upon the nature of the supporting electrolyte and the spacing between the electroactive groups on the polymer chains.

ACKNOWLEDGEMENTS

The cooperation of Johna Leddy in performing some critical final experiments is appreciated. Discussions of the model with Dr. Raymond Jasinski were helpful. The generosity of the Occidental Research Corporation in providing the computer time necessary to finish the simulation is gratefully acknowledged. The support of this work by the National Science Foundation is appreciated.

APPENDIX

Digital simulation of the cyclic voltammetric behavior of multilayer electroactive films on electrodes

Details of the general technique [14] used to simulate cyclic voltammograms for multilayer surface films and a flow chart of the FORTRAN program are given below. The procedure is illustrate for the simple films without interactions. The modifications to this basic set of equations which are required to simulate more complex types of behavior were described above.

The model of Fig. 2 is assumed. The initial conditions are:

$$FCA(J, K) = 1.0 \qquad J = 1\ , JMAX(0 < x < l)$$
$$FCB(J, K) = 0.0 \qquad K = 0 \qquad (t = 0) \tag{A1}$$

where, $FCA(J,K)$ and $FCB(J,K)$ are the fractional concentrations of oxidized and reduced sites, respectively, in the Jth box at the Kth time interval ($K = L$ when $t = \tau$).

The potential scan is initiated and allowed to proceed for a time interval, Δt ($t = \Delta t$, $K = 1$), during which the potential changes by an amount, SC,

$$E = E_S - SC \tag{A2}$$

$$SC = (E_S - E_F)/L = v\Delta t \tag{A3}$$

The resulting current is calculated as shown on next page flow chart.

The forward and backward heterogeneous electron transfer rate constants, RKF and RKB, respectively, are evaluated at E:

$$RKF = RKS \exp[-\alpha\,(nF/RT)(E - E^0)] \tag{A4}$$

$$RKB = RKS \exp[(1 - \alpha)(nF/RT)(E - E^0)] \tag{A5}$$

These values of RKF and RKB are then used to calculate the dimensionless flux, $FLUX$:

$$FLUX = (RKF \cdot FCA(1,1) - RKB \cdot FCB(1,1))/(1 + RKF/2DM + RKB/2DM) \tag{A6}$$

The real current in microamperes is obtained from the dimensionless flux with the equation,

$$i = FLUX \cdot Q \cdot D^{1/2} \cdot v^{1/2}/DM^{1/2} \cdot SC^{1/2} \cdot l \tag{A7}$$

where, Q is the total film charge in microcoulombs, and the units of D, v, and l are $cm^2\ s^{-1}$, $V\ s^{-1}$, and cm, respectively. The fractional concentrations of the oxidized and reduced sites in box 1 are then corrected for electron transfer,

$$FCA(1,1) = FCA(1,1) - FLUX \tag{A8}$$

$$FCB(1,1) = FCB(1,1) + FLUX \tag{A9}$$

It is not necessary to store FCA and FCB for each time interval, since only the values of FCA and FCB at K and $K + 1$ are used during the course of the

Flow chart

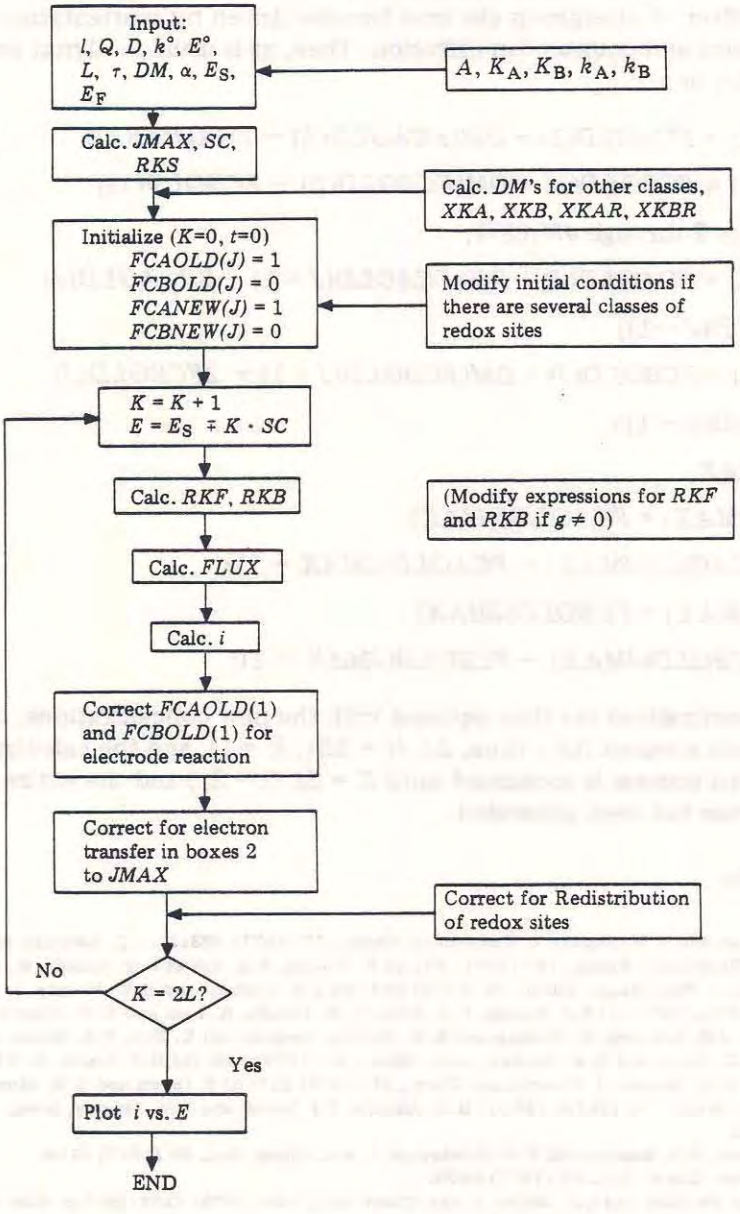

simulation. Thus [14a]:

$$FCAOLD(J) = FCA(J,K) \qquad t = t \tag{A10}$$

$$FCANEW(J) = FCA(J,K+1) \qquad t = t + \Delta t \tag{A11}$$

$FCA(1,1)$ and $FCB(1,1)$ are replaced by $FCAOLD(1)$ and $FCBOLD(1)$, respectively.

Diffusion proceeds outward from box 1 as a result of the concentration gradient created by the electrode reaction in box 1. This process represents the combined effect of intergroup electron transfer driven by reorientation of the polymer chains and counter ion diffusion. Then, as is usual in digital simulations [14] for box 1,

$$FCANEW(1) = FCAOLD(1) + DM(FCAOLD(2) - FCAOLD(1))$$
$$FCBNEW(1) = FCBOLD(1) + DM(FCBOLD(2) - FCBOLD(1)) \quad \text{(A12)}$$

and for boxes 2 through $JMAX$-1,

$$FCANEW(J) = FCAOLD(J) + DM(FCAOLD(J+1) - 2FCAOLD(J) + FCAOLD(J-1))$$
$$FCBNEW(J) = FCBOLD(J) + DM(FCBOLD(J+1) - 2FCBOLD(J) + FCBOLD(J-1)) \quad \text{(A13)}$$

For box $JMAX$,

$$FCANEW(JMAX) = FCAOLD(JMAX) - DM(FCAOLD(JMAX) - FCAOLD(JMAX-1))$$
$$FCBNEW(JMAX) = FCBOLD(JMAX) - DM(FCBOLD(JMAX) - FCBOLD(JMAX-1)) \quad \text{(A14)}$$

the old concentrations are then equated with the new concentrations, the potential is again scanned for a time, Δt, ($t = 2\Delta t$, $K = 1$), and the calculation repeated. This process is continued until $K = 2L$ ($t = 2\tau$) and the entire cyclic voltammogram has been generated.

REFERENCES

1 (a) P.R. Moses and R.W. Murray, J. Electroanal. Chem., 77 (1977) 393; (b) J.R. Lenhard and R.W. Murray, J. Electroanal. Chem., 78 (1977) 195; (c) R. Nowak, F.A. Schultz, M. Umaña, H. Abruña and R.W. Murray, J. Electroanal. Chem., 94 (1978) 219; (d) J.R. Lenhard and R.W. Murray, J. Am. Chem. Soc., 100 (1978) 7870; (e) R.J. Nowak, F.A. Schultz, M. Umaña, R. Lam and R.W. Murray, Preprint; (f) P. Daum, J.R. Lenhard, D. Rolison and R.W. Murray, preprint; (g) K. Kuo, P.R. Moses, J.R. Lenhard, D.C. Green and R.W. Murray, Anal. Chem., 51 (1979) 745; (h) D.F. Smith, K. William, K. Kuo and R.W. Murray, J. Electroanal. Chem., 95 (1979) 217; (i) P. Daum and R.W. Murray, J. Electroanal. Chem., 103 (1979) 289; (j) H.D. Abruña, T.J. Meyer and R.W. Murray, Inorg. Chem., 18 (1979) 3233.

2 H.L. Landrum, R.T. Salmon and F.M. Hawkridge, J. Am. Chem. Soc., 99 (1977) 3154.

3 A. Diaz, J. Am. Chem. Soc., 99 (1977) 5838.

4 (a) M.R. Van De Mark and L.L. Miller, J. Am. Chem. Soc., 100 (1978) 3223; (b) J.B. Kerr and L.L. Miller, J. Electroanal. Chem., 101 (1979) 263.

5 (a) K. Itaya and A.J. Bard, Anal. Chem., 50 (1978) 1487; (b) A. Merz and A.J. Bard, J. Am. Chem. Soc., 100 (1978) 3222; (c) P.J. Peerce and A.J. Bard, J. Electroanal. Chem., 108 (1980) 121.

6 (a) M.S. Wrighton, R.G. Austin, A.B. Bocarsly, J.M. Bolts, O. Haas, K.D. Legg, L. Nadjo and M.C. Palazzotto, J. Am. Chem. Soc., 100 (1978) 1602; (b) J. Electroanal. Chem., 87 (1978) 429; (c) J.M. Bolts and M.S. Wrighton, J. Am. Chem. Soc., 100 (1978) 5257; (d) M.S. Wrightin, M.C. Pallazzotto, A.B. Bocarsly, J.M. Bolts, A.B. Fischer and L. Nadjo, J. Am. Chem. Soc., 100 (1978) 7264; (e) J.M. Bolts, A.B. Bocarsly, M.C. Pallazzotto, E.G. Walton, N.S. Lewis and M.S. Wrighton, J. Am. Chem. Soc., 101 (1979) 1378; (f) A.B. Bocarsly, E.G. Walton, M.G. Bradley and M.S. Wrighton, J. Electroanal. Chem., 100 (1979) 283.

7 (a) F.B. Kaufman and E.M. Engler, J. Am. Chem. Soc., 101 (1979) 547; (b) F.B. Kaufman, A.H. Schroeder, E.M. Engler, S.R. Kramer and J.Q. Chambers, preprint.
8 (a) N. Oyama and F.C. Anson, J. Am. Chem. Soc., 101 (1979) 739; (b) ibid., 3450; (c) J. Electrochem. Soc., 127 (1980) 247.
9 R.F. Lane and A.T. Hubbard, J. Phys. Chem., 77 (1973) 1401.
10 (a) H. Angerstein-Kozlowska and B.E. Conway, J. Electroanal. Chem., 95 (1979) 1; (b) H. Angerstein-Kozlowska, J. Klinger and B.E. Conway, J. Electroanal. Chem., 75 (1977) 45; (c) E. Laviron, J. Electroanal. Chem., 101 (1979) 19; (d) V. Plichon and E. Laviron, J. Electroanal. Chem., 71 (1976) 143 and references therein.
11 Y-H. Chen, M. Fernandez-Refojo and H.G. Cassidy, J. Polymer Sci., 40 (1959) 433.
12 J.C. Lai, T. Rounsfell and C.U. Pittman, J. Polymer Sci. A-1, 9 (1971) 651.
13 P.G. de Gennes, Nature, 282 (1979) 367.
14 (a) A.J. Bard and L.R. Faulkner, Electrochemical Methods, Wiley, New York, 1980, Appendix B; (b) S. Feldberg, in A.J. Bard, (Ed.), Electroanalytical Chemistry, Vol. 3, Marcel Dekker, 1969, p. 199.
15 Yu.S. Lipatov and L.M. Sergeeva, The Adsorption of Polymers, Wiley, New York, 1974, Ch. 1.
16 C.A.J. Hoeve, J. Chem. Phys., 43 (1965) 3007.
17 (a) C.D. Jaeger, Ph.D. Thesis, The University of Texas at Austin, 1979; (b) T. Henning, unpublished experiments, 1979.
18 C.D. Jaeger and A.J. Bard, J. Am. Chem. Soc., 101 (1979) 1690.